IEEE Access
Multidisciplinary ⋮ Rapid Review ⋮ Open Access Journal

Received 6 October 2023, accepted 19 October 2023, date of publication 27 October 2023, date of current version 6 November 2023.

Digital Object Identifier 10.1109/ACCESS.2023.3328143

RESEARCH ARTICLE

Advanced Design Optimization of Switched Reluctance Motors for Torque Improvement Using Supervised Learning Algorithm

MOHAMED OMAR[1,2], (Graduate Student Member, IEEE), MOHAMED H. BAKR[1], (Senior Member, IEEE), AND ALI EMADI[1], (Fellow, IEEE)

[1]Department of Electric and Computer Engineering, McMaster University, Hamilton, ON L8S 4L8, Canada
[2]Department of Power Electronics and Energy Conversion Systems, Electronics Research Institute, Cairo 11796, Egypt

Corresponding author: Mohamed Omar (omarm8@mcmaster.ca)

ABSTRACT Existing research on geometry optimization of switched reluctance motor (SRM) using machine learning algorithms has focused only on the machine's static characteristics. The dynamic characteristics, however, are critical to improve the SRM performance, particularly at high speeds. This paper introduces an advanced optimization method utilizing a supervised learning algorithm to act as a surrogate model for both static and dynamic characteristics of the SRM. In this work, back-propagation neural network (BPNN) is applied to map out the SRM geometrical parameters, stator and rotor pole arc angles and their dynamic performance metrics such as average torque and torque ripples. To capture the training data, finite element analysis (FEA) and MATLAB Simulink models are implemented to study the static and dynamic characteristics of the considered 6/14 SRM. Levenberg-Marquardt is applied to train the BPNN. The results of the proposed optimal design candidates are verified using FEA and MATLAB simulations, confirming the effectiveness of the optimal design. The optimal design improves the average torque by around 2% and reduces the torque ripples by around 24%. Moreover, the proposed method significantly decreases the computational overhead.

INDEX TERMS Electric motor design, machine learning (ML), supervised learning, switched reluctance motor (SRM).

I. INTRODUCTION

Switched reluctance motors (SRMs) are gaining popularity due to their uncomplicated and robust structure, which does not include any magnets or windings in the rotor [1]. The absence of permanent magnets and rotor windings enables the SRM to operate efficiently at high temperatures and speeds [2]. This design feature also results in a lighter rotor, leading to a higher torque-to-inertia ratio and improved dynamic performance as compared to induction machines (IMs) and permanent magnet synchronous motors (PMSMs) [3]. Furthermore, the SRM's lack of rare-earth material makes it a cost-effective alternative to PMSMs.

Despite these potential benefits, this motor still faces some drawbacks that hinder wide industrial applications. The structure of SRMs, with its doubly salient nature, poses certain challenges, such as significant torque ripples, acoustic noise, and vibrations [4]. Another primary concern is the complexity of modeling SRMs because of its highly nonlinear characteristics. Also, the need for uncommon converters for driving this motor is another weakness. To address these challenges and enhance the motor's static and dynamic performance, extensive research was conducted.

SRM geometry optimization has been employed to improve machine performance and address design challenges. Geometry optimization requires predicting the performance of SRMs across all magnetic circuit parameters for certain operating conditions [5], [6]. Lumped parameter models have been employed in the literature for the machine's

The associate editor coordinating the review of this manuscript and approving it for publication was Wei Liu.

preliminary sizing and analysis. Using these methods within an optimization procedure results, however, in imprecise outcomes [7]. The advancement of computer hardware and software facilitated the utilization of finite element analysis (FEA) for multi-objective optimization, which involves representing a precise magnetic circuit geometry [8], [9]. However, utilizing a time step FEA within an optimization procedure for electric machines results in prohibitive execution time [7], [10].

Moreover, integrating SRM dynamic simulations into FEA software poses challenges due to the need to incorporate a power electronics inverter requiring a current controller [11]. The current controller generates switching signals that, in turn, are supplied to the inverter for switching the DC-link voltage thus regulating the phase current [1]. Executing these tasks within FEA software is computationally expensive.

Generally, the conventional design process for the electromagnetic aspect of SRMs is an iterative, multi-stage process. Initially, a static analysis using FEA is conducted to create look-up tables that map the characteristics of flux linkage and static torque with respect to various rotor positions and currents. Subsequently, dynamic analysis is conducted via MATLAB simulations using the generated look-up tables. Conduction angles optimization is then performed for each geometry design candidate to enhance the dynamic performance. This process is repeated until an optimal design is achieved [12], resulting in a significant execution time for both static (FEA) and dynamic (MATLAB) analyses [13].

Recently, Machine Learning algorithms (MLAs) have gained significant attention in the field of motor design due to their ability to learn from data and generate accurate predictions. MLA can be used to map out the nonlinear profiles of the motor parameters and the output performance. In the context of PMSM, previous studies (e.g. [7], [14]) have successfully utilized extreme learning machine and support vector regression approaches for geometry optimization. Similarly, in [15], a Bayesian regularization back-propagation neural network was introduced to address the geometry optimization challenges of synchronous reluctance motors.

Focusing on the SRM, which is the primary scope of this study, a generalized regression neural network (GRNN) was developed to optimize the pole arc angles of 12/8 SRM in [16]. To analyze the static characteristics, an FEA model was implemented, and the GRNN was utilized as a surrogate model to represent these static characteristics [16]. However, it is important to note that this work is limited to low-speed operations of SRMs. In [17], another study introduced the utilization of GRNN for modeling a 12/8 SRM. The aim was to capture the nonlinear correlations between motor performance against rotor yoke and pole arc angles. The sample data used in this study, however, was only based on FEA static analysis. Moreover, this approach involves designing two separate GRNN structures to predict the motor performance, which added complexity to the design process. The developed approach in [17] did not estimate new geometrical parameters that could potentially enhance motor performance. It is important to highlight that both previous studies, [16], [17], lack the consideration of SRM dynamic characteristics and conduction angles optimization.

This paper introduces an advanced optimization approach that harnesses the power of a supervised learning algorithm to accurately model both the static and dynamic characteristics of 6/14 SRM. Specifically, we have adopted a Back-Propagation Neural Network (BPNN) to study the impact of variations in stator and rotor pole arc angles on the machine's static and dynamic performance. The Levenberg Marquardt (LM) algorithm has been utilized in this study to ensure fast and efficient learning of the BPNN. The dynamic modeling incorporates the utilization of a genetic algorithm for conduction angles optimization, thereby enhancing the torque performance of the considered SRM. As a result, the proposed method not only acts as a surrogate for the machine's static characteristics but also effectively models its dynamic behavior, including the optimization of conduction angles.

Our proposed methodology is evaluated using various performance metrics, and the results are compared with those of traditional design methods. The findings of this study demonstrate the effectiveness and efficiency of ML-based approaches in SRM design. Moreover, this method demonstrates a substantial reduction in computational time and costs in comparison to traditional iterative techniques.

The rest of the paper is structured as follows: Section II explores the impact of the design parameters, specifically the pole ac angles, on the motor performance. Section III introduces the utilized approach to acquire the training data. In Section IV, the structure of the proposed BPNN and its evaluation approach are presented. Section V then focuses on the generation of new design candidates, followed by an analysis and selection of the optimal design candidate. Finally, concluding remarks are listed in Section VI to summarize the findings and implications of the study.

II. POLE ARC ANGLES DESIGN EFFECT AND CONSTRAINTS

Generally, the SRM pole arc angles are carefully selected. Increasing the stator pole arc angle, β_s, widens the stator teeth increases the aligned flux linkage and extends the SRM torque angle at each pulse which might cause lower torque ripples. The excessive increase in β_s, however, can reduce the motor saliency, thus decreasing the peak and RMS of the output torque [18]. Moreover, a larger β_s can compress the winding space, and this can reduce the number of turns, which leads to a torque reduction [18]. Similar to β_s, slightly increasing rotor arc angle, β_r, widens the rotor teeth and would boost the aligned flux linkage which enhances the output torque. Also, the excessive increase in β_r would reduce the motor saliency, and as a result, the output torque production can be decreased [18]. Therefore, the design of the SRM pole arc angles is sensitive and crucial.

The approach focuses on maximizing the average torque based on the pole arc angles variations. In SRMs, pole arc angles have a powerful effect on the inductance and torque quality profiles. Electromagnetic torque production is contingent on the changes in magnetic reluctance. To ensure this, the design of the length of the stator and rotor pole arcs should guarantee a fully unaligned position. Otherwise, the rotor tooth of the SRM will partially or totally align with the stator tooth at any rotor position. Therefore, to maintain this condition, the stator tooth arc length should be lower than the arc length between two successive rotor teeth [1]. This condition defines the maximum values of β_s and β_r. Furthermore, the minimum values of β_s and β_r should guarantee the self-starting capability of SRMs [1]. The applied constraints of β_s and β_r are identified in (1) for the given number of phases, m and rotor poles, Nr [19]. Based on these constraints, the range of possible combinations of β_s and β_r is [8.57:12.85]. These bounds are given by:

$$\frac{4\pi}{mN_r} \leq \beta_s + \beta_r < \frac{2\pi}{N_r} \tag{1}$$

III. TRAINING DATA ACQUISITION

To effectively model and design an SRM using an MLA, it is crucial to accurately capture sample data that depicts the correlation between the input design parameters variation and the corresponding output objectives. Electromagnetic modeling is thus conducted to study the static analysis of the considered SRM. Following that, a dynamic analysis is carried out to determine the output objectives for each design candidate. This dynamic model includes conduction angles optimization to ensure optimal performance. In this section, we present a detailed explanation of the static and dynamic modeling required to generate the required training data.

A. FINITE ELEMENT MODELING

Electromagnetic modeling forms the basis of SRMs geometrical design optimization. The modeling methods can be categorized into numerical and analytical approaches [13]. Analytical-based modeling methods are possibly used in the static analysis of SRMs. However, they commonly require various assumptions, which are not usually easy to provide [20]. These approaches do not accurately account for motor nonlinearities [1]. Therefore, in this study, we employ a numerical FEA-based modeling method, which is recommended for static characterization of SRMs [1]. FEA is the most widely used numerical modeling method. The FEA model is applied to characterize the static flux linkage and static torque profiles of the 3-ph 6/14 SRM at different rotor positions and phase currents. The major geometrical parameters of the base design of the 6/14 SRM are summarized in Table 1, and its full FEA JMAG model is shown in Fig. 1.

The study of static phase characteristics is pivotal for understanding the operational principles and nonlinear behavior of the switched reluctance machines. In this research, the static characteristics of the considered SRM are

TABLE 1. Parameters of the considered 6/14 SRM.

Parameter	Symbol	Value
DC-link Voltage [V]	VDC	163
Stack length [mm]	L	74
Stator outer diameter [mm]	D_s	139.21
Shaft diameter [mm]	D_{sh}	12.7
Air gap length [mm]	L_g	0.4
Stator back iron thickness [mm]	y_s	10
Rotor back iron thickness [mm]	y_r	35.78
Stator pole height [mm]	h_s	10
Rotor pole height [mm]	h_r	7.08
Stator pole arc angle [°]	β_s	9.5
Rotor pole arc angle [°]	β_r	9.3
Stator taper angle [°]	τ_s	4
Rotor taper angle [°]	τ_r	4

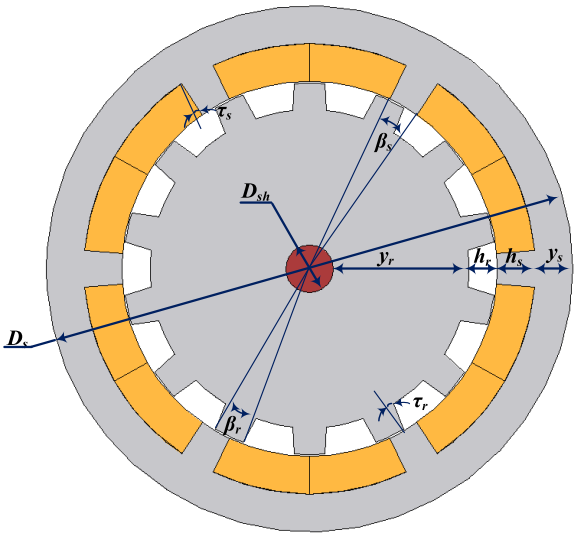

FIGURE 1. The FEA JMAG full model of the considered 6/14 SRM.

referred to as the flux linkage, induced voltage, and phase torque when a single phase is excited by a constant current over the entire electrical cycle. This is because the mutual coupling among phases is neglected in this work.

In traditional configurations of switched reluctance machines, which possess an even number of stator poles per phase, as is the case with the SRM under investigation in this study, mutual coupling occurs momentarily during each cycle. Generally, this effect can be disregarded when formulating a model for an SRM [1]. This is because when current is applied to the coils of a typical SRM phase, the bulk of the resulting magnetic flux is interlinked with the

coils of the very same phase. Hence, in FEA conducted in this research, a single phase is energized with a constant current throughout one complete electrical cycle.

Subsequently, we relatively increased the static current applied to energize the phase to simulate the impact of core saturation. The static flux linkage and torque profiles at various rotor positions and phase currents are depicted in Figs. 2 and 3, respectively. Fig. 2 illustrates that the incremental rise in the flux linkage diminishes at high currents due to the elevated magnetic flux density, resulting in a higher level of core saturation. Furthermore, it is worth noting that the look-up tables (LUT) created for one phase can be effectively employed to model all phases.

To cover the entire design domain while adhering to the given constraints, 50 different configurations with appropriate pole arc angles are considered. The static characteristics of each SRM design are then imported into a MATLAB/Simulink model for dynamic analysis. The dynamic analysis provides the average torque and torque ripples values for each design candidate for performance assessment.

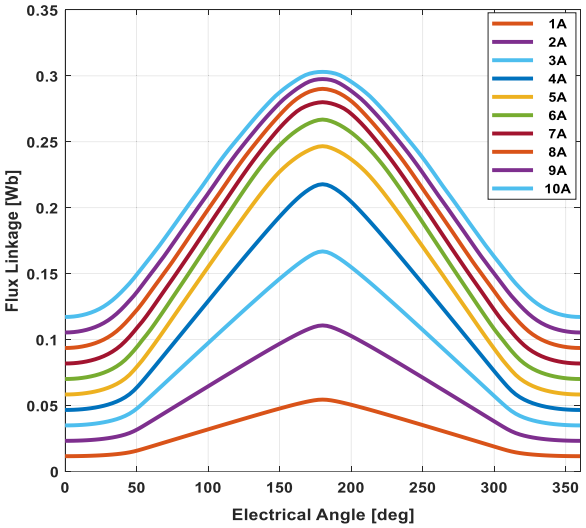

FIGURE 2. The static flux linkage characteristics of the 6/14 SRM at various rotor positions and phase currents.

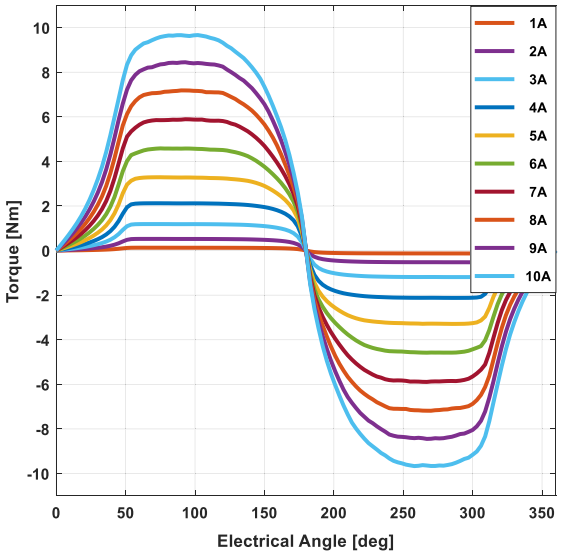

FIGURE 3. Static torque profiles of 6/14 SRM at various rotor positions and phase currents.

B. DYNAMIC MODELING

In contrast to PMSMs and IMs, SRMs do not operate with sinusoidal currents. The switching nature of the SRM magnetic field makes it challenging to directly apply phase transformation techniques to drive SRMs [1]. Consequently, SRMs require distinct modeling approaches to study their dynamic behavior. The developed dynamic model in this work assesses the motor's performance while operating at a constant speed considering the dependency of the flux linkage on the current and rotor position. This dynamic model computes the dynamic average torque and torque ripples by exciting the phase for given firing angles, motor speed, and DC link voltage.

In this section, we explain the utilized MATLAB Simulink model and how it exploits the offline phase flux linkage LUT generated from FEA simulations. The model is primarily built based on the voltage equation (2), which relates the SRM phase voltage, v_{ph} to the phase current, i_{ph}, and flux linkage, λ_{ph} [21]:

$$v_{ph} = R_{ph} i_{ph} + \frac{d\lambda_{ph}(i_{ph}, \theta_{ph})}{dt} \tag{2}$$

The Simulink model of the SRM is formulated as a discrete-time domain with a fixed time step. Solving (2) for the flux linkage in discrete time domain form and look up the current based on the past flux values, we get:

$$\lambda_{ph}(k) = \lambda_{ph}(k-1) + [v_{ph}(k) - R_{ph} i_{lut}(\lambda_{ph}(k-1), \theta_{elec}(k-1))]T_s \tag{3}$$

where k is the discrete step value and T_s is the sampling time. i_{lut} is the current required to get a specific flux linkage at a certain electrical angle, θ_{elec}. This i_{lut} can be derived from the inversion of the phase flux linkage LUT. Using (3), a dynamic simulation model can be implemented to solve for the SRM flux linkage and current. The calculated current waveform can then be employed to evaluate the torque, as depicted in Fig. 4.

The dynamic model of the SRM also includes the angle model and hysteresis current controller model. The correlation between the SRM phase voltage and current relies on the current control method, with the current being regulated by an asymmetric bridge converter and various control parameters. Typically, the primary control parameters are the reference current and turn-on and turn-ff angles, which are utilized to generate the commanded current for phase current regulation. Hysteresis control is applied in

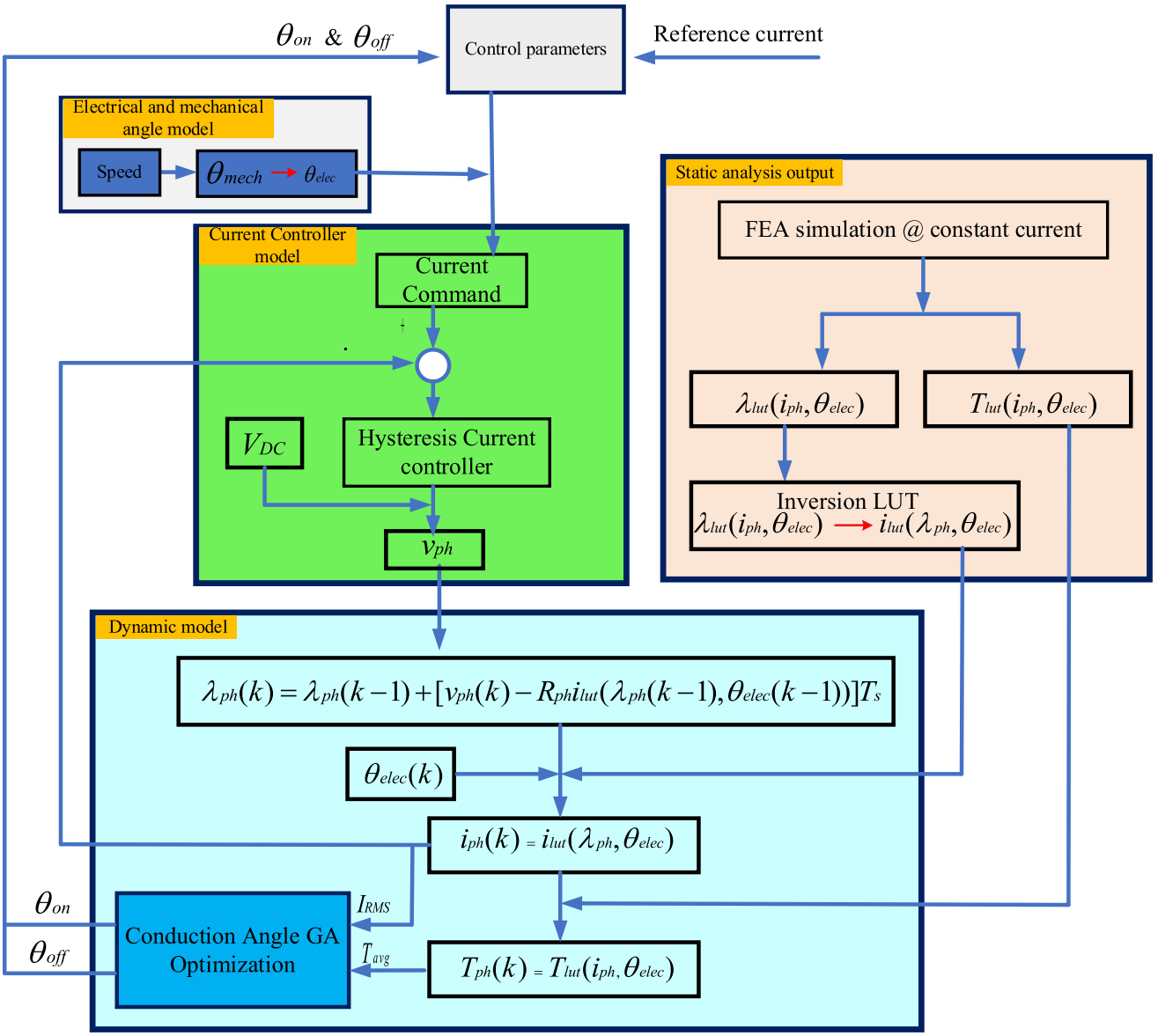

FIGURE 4. A simplified chart for the developed dynamic model for the considered SRM.

SRM drives to maintain tracking of the reference current. When the phase current achieves the reference current value, the hysteresis controller maintains it within the predefined hysteresis band. Fig. 4 shows a simplified chart for the developed dynamic model.

C. CONDUCTION ANGLE OPTIMIZATION

The current control at low speeds can track the reference current to achieve the proposed torque, while the conduction angles can decrease the ripples and enhance motor efficiency [1]. On the other hand, tracking the peak current at high speeds is not attainable due to the high induced voltage. In such cases, the conduction angles would be the sole control parameters. Therefore, to enhance the SRM performance at various operation conditions, the selection of conduction angles, turn-on, θ_{on} and turn-off, θ_{off} angles, should be made with utmost precision.

Tuning the conduction angles manually for each geometrical design candidate is considerably time-consuming [1]. Therefore, in this paper, an optimization algorithm based on a Genetic Algorithm (GA) is applied to speed up getting the optimal candidate firing angles. The main objective used in the developed genetic optimization algorithm is maximizing the average torque, T_{avg},

$$f_{obj} = T_{avg} = \frac{1}{\theta_{cycle}} \int_{0}^{\theta_{cycle}} T(\theta) d\theta \tag{4}$$

The average torque is determined based on the instantaneous phase torque, $T(\theta)$ over one complete electrical cycle, θ_{cycle}.

Linear constraints are set for the range of the θ_{on} and θ_{off} to effectively cover the operation within the application design space [12]. A nonlinear constraint is set for the phase RMS current, I_{RMS}, that is calculated based on the instantaneous phase current, *Iph* as follows:

$$I_{RMS} = \sqrt{\frac{1}{\theta_{cycle}} \int_{0}^{\theta_{cycle}} i_{ph}^2(\theta) d\theta} \leq I_{RMS\_constraint} \quad (5)$$

After running the FEA simulation using JMAG software for the base design of the considered SRM, the generated LUTs are implemented in the developed dynamic SIMULINK model and executed at the base speed, 1103RPM. The θ_{on} and θ_{off} are optimized to maximize the average torque. The dynamic model was executed so that the initial two cycles were designated as transient periods, and the subsequent cycles were employed for the calculation of average torque and torque ripples. The average torque per phase and total torque of the third electrical cycle are shown in Fig. 5.

In order to capture the complete necessary training data, a parametric sweep was conducted for the pole arc angles while considering the previously mentioned constraints. This resulted in the acquisition of 50 design candidates. Following this, FEA analysis was carried out, and the Flux linkage and average torque LUT were imported to the SRM dynamic drive model. For each design candidate, the conduction angles were optimized using the GA to achieve maximum average torque. Therefore, the trained MLA not only acts as a surrogate for the FEA analysis but also for the dynamic model, including the GA optimization of the conduction angles.

To ensure the quality of the output torque, the RMS value of the torque ripple is determined, in eq. (6), using the developed dynamic model. The torque ripple of each design candidate is also utilized as a second output for the MLA. For example, Table 2 shows 5 samples out of the 50 samples that were used to train the developed MLA. The MLA can thus predict the average torque and torque ripples for any new SRM pole arc angles. This facilitates the selection of the optimal design candidate considering both the net output torque and torque quality.

$$\Delta T_{RMS} = \sqrt{\frac{1}{\theta_{cycle}} \int_{0}^{\theta_{cycle}} (T(\theta) - T_{avg})^2 d\theta} \quad (6)$$

To validate the developed dynamic model, the three phase current waveforms of the baseline design which were computed within the MATLAB dynamic model, shown in Fig. 6, are imported into the FEA static model of the SRM. Subsequently, we compared the torque waveforms generated by the dynamic model and the FEA model. The comparison, as illustrated in Fig. 7, reveals a close match between the torque waveforms. It is important to emphasize that mutual coupling was not considered in the dynamic model,

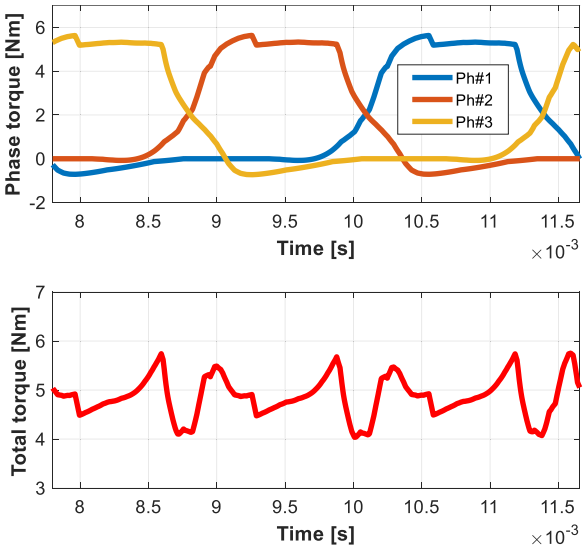

FIGURE 5. The phase and total average torque of the base design of the considered SRM.

TABLE 2. Some examples of the training data.

β_s	β_r	Average torque	Torque ripples (ΔT_{RMS})
8.5	9	4.688	0.413
9	9	4.736	0.367
9	10	4.897	0.311
9.5	9	4.832	0.399
9.5	10	5.024	0.428

whereas the FEA simulations inherently account for mutual coupling effects. The strong agreement between the results underscores the insignificance of mutual coupling when modeling this SRM drive with the optimized firing angles. It should be highlighted that the validation process using the FEA demands a substantially longer computational time as compared to the established dynamic model. This observation emphasizes the significance of dynamic modeling as an efficient and practical approach for our study.

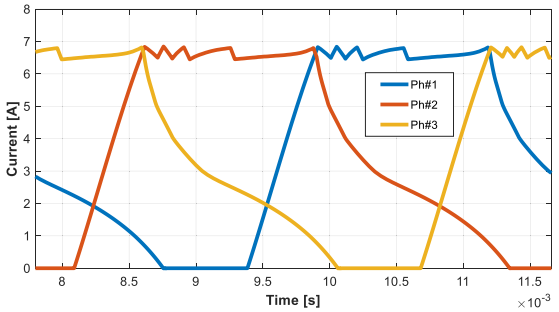

FIGURE 6. Three phase dynamic currents of the baseline design of the considered SRM at base speed and peak reference current (6.66A) and for $\theta_{on} = -30.5°$ and $\theta_{off} = 137.47°$.

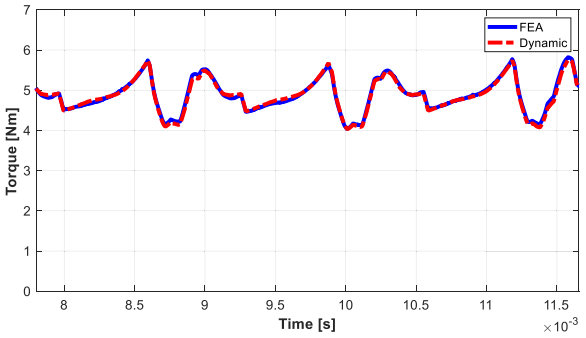

FIGURE 7. A comparison of torque calculated from the FEA and dynamic models for the baseline design.

IV. NEURAL NETWORK STRUCTURE AND EVALUATION

Because of the highly nonlinear characteristics of the SRM, a continuous search within the design domain is necessary for accurate geometry design optimization [16]. However, the acquired training data are discrete points in the design space as presented in the previous section. Simply using a mathematical formula to fit these discrete data will be complicated and inadequate to achieve accurate modeling results [16]. An advantage of using MLA is its ability to predict the nonlinear characteristics of SRM flux linkage and torque profiles from limited data [13].

MLA can be divided into three categories; supervised, unsupervised and reinforcement learning. These learning styles vary in terms of the captured sample data, as well as how it is gathered and evaluated [13]. Among these categories, supervised learning techniques are widely used for modeling and designing electric motors [7], [13], [14], [15], [16], [17]. Therefore, in this study a supervised learning algorithm, especially the BPNN, has been employed.

BPNN commonly uses the gradient decent algorithm (GDA) to minimize the cost function. However, its delayed convergence is the main drawback [22]. Newton's method was used to overcome the GDA's drawback. Newton's method suffers though from the high computational overhead due to the necessity to calculate the Hessian matrix [23]. In this work, the Levenberg Marquardt (LM) is used to train the BBPN, addressing the shortcomings of the Newton and GDA methods. Furthermore, LM ensures the local minimum convergence.

The main aspects of selecting a certain type of neural network include the computation time, generalization capability and fitting accuracy. Typically, the BPNN and the radial basis function neural network (RBFNN) are the most popular neural network types. The computational scale of the network can be determined by the number of hidden layers and neurons. Reducing these numbers is critical in minimizing the computational burden [23]. Additionally, the size of the neural network (NN) model is a crucial factor for real-time applications, such as motor drive controllers [23]. The RBFNN excels at convergence speed and approximation, but it has a larger modeling error, which requires a larger network size than the LM-BPNN. The adoption of LM learning algorithm improved the accuracy of the BPNN and reduced the network scale, which are critical for any NN design. Thus, in this work, LM-BPNN is used for the geometrical design optimization of the considered SRM.

Fig. 8 displays the structure of the BPNN, consisting of two inputs for β_s and β_r and two outputs for the average torque and torque ripples. This BPNN has only one single hidden layer, utilizing Tansig as the activation function for its hidden neurons. The number of optimal hidden nodes was identified as 8. The output layer uses a linear activation function for both outputs.

The decision to employ one hidden layer with eight neurons was determined through a heuristic approach. It balances the tradeoff between the training accuracy and model complexity. Increasing the number of layers or nodes, the training accuracy may improve, but there is a higher likelihood of overfitting. Overfitting indicates that the model structure is complex and fails to achieve an optimal fit with new data. It occurs when the gap between training and test errors becomes substantial, resulting in a notable generalization error [13]. In this section, the generalization capability has been assessed using a small sample size to test the overfitting and ensure the proper design of the BPNN.

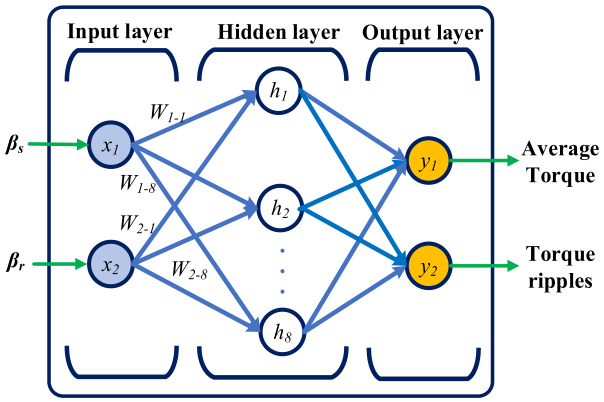

FIGURE 8. The basic architecture of a single-layer BPNN comprises 8 hidden neurons to model the considered 6/14 SRM.

LM algorithm was employed as the optimization algorithm to train the BPNN. To assess the network's performance, the mean square error (MSE) was used as the loss function with a target error set at 0.0001. Additionally, the linear regression correlation coefficient (R) served as another metric for evaluating the fitting accuracy and the precision of the test set [23]. The total number of points in the dataset is 50 points. The division of the dataset involves allocating 70% of the points for training, 15% for validation, and the remaining 15% for testing the network.

The LM algorithm successfully trained the network in 17 epochs. Fig 9. shows the error convergence curve for training, validation, and testing respect to the number of epochs. The training set's MSE is 2.706e-4 Nm, and the linear regression correlation coefficient R is 0.99997. As the MSE is a relatively small value and R is very close to 1, the BPNN

exhibits an excellent degree of precision in representing the nonlinear characteristics of the considered SRM.

After successfully training the BPNN, its generalization capability was evaluated using 10 data points that were not involved during the training or testing phases. The estimated outputs of the BPNN were then compared against the actual average torque and torque ripples. The MSE for these 10 samples is 5.646e-4 Nm, with the corresponding performance indicator R equals 0.977. Additionally, the mean relative error (MRE) of this test dataset is 2.244%. These results demonstrate the high accuracy of the designed BPNN in predicting new data points, validating its capability for effective generalization without encountering overfitting or underfitting issues.

The superiority of the proposed BPNN has been verified through a rigorous comparison with quadratic regression fitting method. While the quadratic regression model demonstrates training data fitting accuracy similar to that of the BPNN, it encounters challenges in achieving a satisfactory level of accuracy when predicting new data. Specifically, the MSE for the training dataset is 2.94e-04, while for the testing dataset, the MSE and MRE are substantially higher at 475.5e-4 and 25.822%, respectively.. This considerable gap between the training and testing results for the quadratic regression method clearly signifies the presence of an overfitting problem. In contrast, the proposed BPNN showcases its remarkable capability to predict new data with exceptional accuracy, highlighting its superior performance and versatility in modeling and forecasting SRM behavior.

V. ESTIMATION, ANALYSIS AND SELECTION OF OPTIMAL DESIGN CANDIDATES.

Following the training and evaluation of the BPNN, it was utilized to generate 10,000 new design candidates that were not previously utilized for network training or testing. The BPNN's outcomes are visualized in a 2-D plane, as shown in Fig. 10, where the objectives, namely the average torque and the torque ripples, are plotted for each design candidate. From the results obtained, two design candidates, identified as DC1 and DC2, were chosen as optimal candidates, as shown in Fig. 10. DC1 has the highest average torque, whereas DC2 has the lowest torque ripples. The design variables and the performance objectives of the optimized design candidates are compared to the base design. The comparison outcomes are presented in Table 3.

A. VERIFICATION OF BPNN RESULTS

To verify the estimated output of the neural network, both static and dynamic analyses were carried out. The actual values of the average torque and torque ripples were compared to the BPNN estimated values, as shown in Table 4. The relative error of the average torque of DC1 and DC2 is 0.05% and 0.36%, respectively. Also, the relative error of the RMS torque ripples of DC1 and DC2 is 2.10% and 0.03%, respectively. These extremely low error values reflect the precision of the proposed BPNN model.

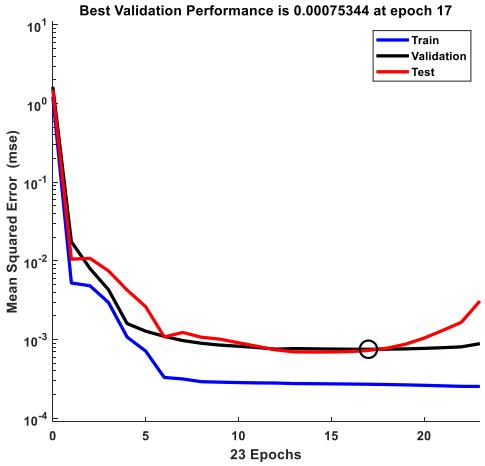

FIGURE 9. The train, validation, and testing profiles of the BBNN.

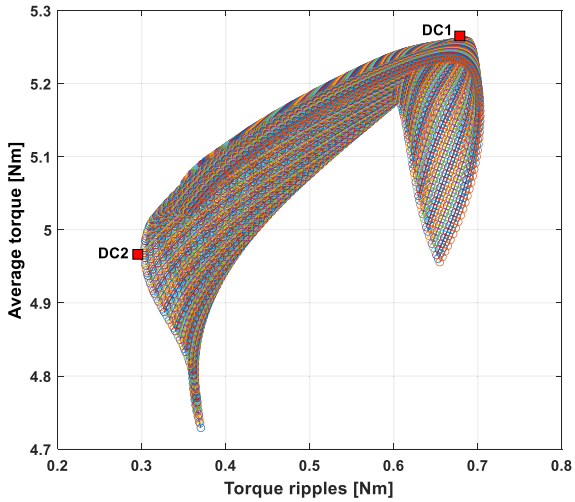

FIGURE 10. A scattered 2–D plane showing the objective outputs of 10,000 design candidates generated by the trained BPNN. The two recommended designs are identified as DC1 and DC2.

TABLE 3. The design variables and performance objectives of the baseline and optimized design candidates.

Parameter	Baseline	DC1	DC2
β_s [°]	9.5	10.8788	9.00
β_r [°]	9.3	11.1212	10.7273
Average torque [Nm]	4.88	5.2585	4.9687
Torque ripples [Nm]	0.398	0.6857	0.3032

B. ANALYSIS OF OPTIMAL DESIGN CANDIDATES

To investigate BPNN-estimated design candidates, FEA JMAG models of DC1 and DC2 were simulated using their proposed pole arc angles. Fig. 11 illustrates the partial cross-sectional models of the baseline and optimized design candidates. The static torque profiles of DC1 and DC2

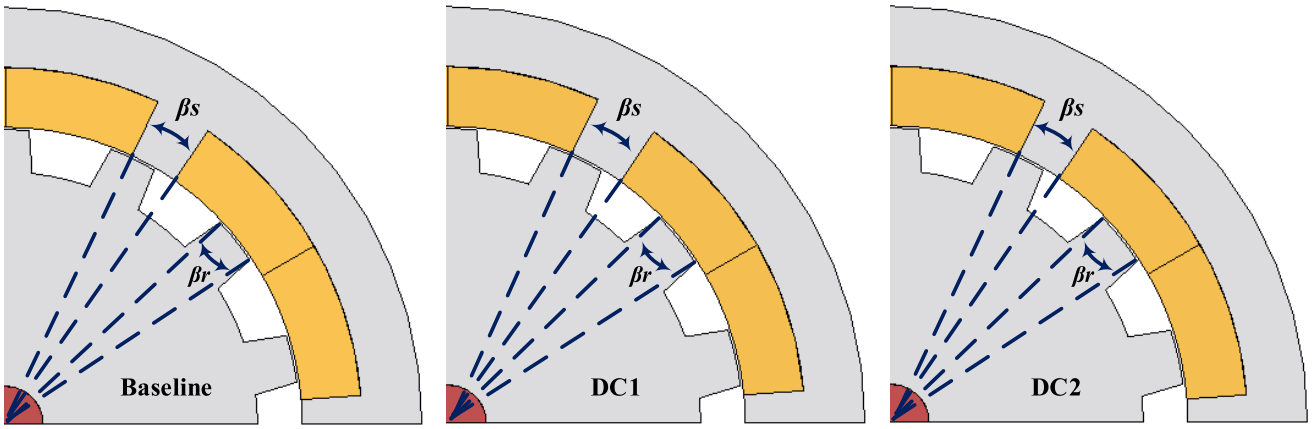

FIGURE 11. FEA JMAG partial model of the baseline and the optimized design candidates.

TABLE 4. The actual and estimated values of the average torque and torque ripples of the optimized design candidates.

Parameter	DC1		DC2	
	BPNN	Actual	BPNN	Actual
Average torque [Nm]	5.2585	5.2610	4.9687	4.9865
Torque ripples [Nm]	0.6857	0.6716	0.3032	0.30329

TABLE 5. Conduction angles of baseline and optimized design candidates.

Conduction Angles	Baseline	DC1	DC2
Turn ON, θ_{on} [°]	-30.5	-36.9	-29.2
Turn OFF, θ_{off} [°]	137.47	131.1	138.7

compared to the baseline at different phase currents are shown in Fig. 12 and Fig. 14, respectively. Whereas the dynamic torque output for a complete electrical cycle of both design candidates is shown in Fig.13 and Fig. 15. Notably, enlarging the stator pole arc angles in DC1 causes a fast rise for the static torque profile. Thus, the total motor torque output from the dynamic SIMULINK model is increased as shown on the blue graph in Fig. 12.

In addition to the analysis of the static behavior of the optimized design candidates, we also assessed their dynamic characteristics, particularly the optimization of conduction angles, to validate the performance of the BPNN output. In DC1, the optimized turn-on angle of the current is more advanced than in DC2, as indicated in Table 5. Advancing the turn-on angle leads to injecting the current before the build-up of the induced voltage, resulting in an increase in the total average torque produced. Thus, DC1 experienced higher average torque than DC2. Although DC1 recorded the highest average torque, it also exhibited a greater value of RMS torque ripples. Because the conduction angle optimization is a single-objective process aimed at maximizing the average torque, even if it comes at the expense of higher torque ripples. Future work will include multi-objective optimization to promote the SRM average torque and torque quality. It is evident that the proposed BPNN has accurately surrogated the optimization process of the conduction angles which saved a significant computational time.

In SRM with a larger number of rotor poles, proximity between the poles results in flux leakage to adjacent poles during phase energization. As the adjacent pole experiences a declining inductance profile, it is reasonable to anticipate a negative torque output [19]. This leads to increased torque ripples, negatively impacting the motor's torque quality. To address this issue, one solution is to widen the rotor-pole arc angle compared to the stator-pole arc angle. This intentional difference introduces dead time in the inductance profile during turn-off delay, preventing potential negative torque during phase conduction and promoting self-starting capabilities [24]. In this study, both design candidates, DC1 and DC2, demonstrate a larger rotor pole arc angle compared to the stator pole arc angle. However, the difference between β_r and β_s in DC2 is significantly greater than in DC1. This increases the dead zone in the middle of the static torque waveform in DC2 compared to DC1, as shown in Fig. 12 and Fig. 14. This eliminates the negative torque production and hence reduces the torque ripples more effectively in DC2 compared to the baseline and DC1 designs. Consequently, by reducing the torque ripples, the overall torque quality is improved, leading to a reduction in audible noise generation from the SRM.

The recommended designs meet the arc angles constraints and are deemed as effective solutions with respect to the output performance of the considered SRM. However, since both design candidates exhibited an average torque slightly higher than the baseline, the selection of the best candidate was prioritized based on its output torque ripples. Consequently, DC2 was selected as the most optimal design candidate as it exhibited an average torque enhancement of

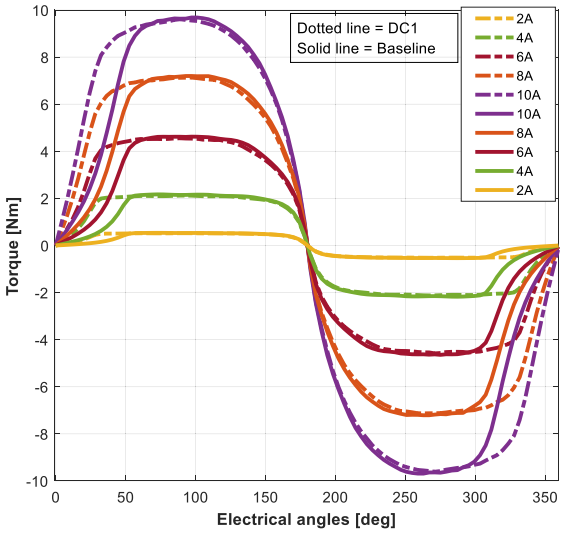

FIGURE 12. Static torque profiles comparison between DC1 and baseline at various phase currents.

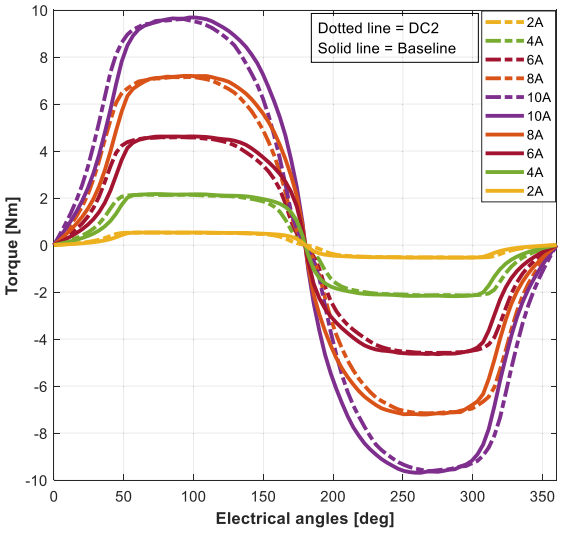

FIGURE 14. Static torque profiles comparison between DC2 and baseline at various phase currents.

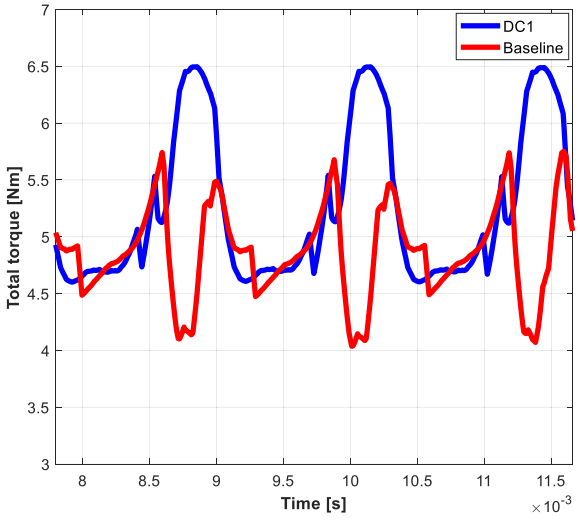

FIGURE 13. Total torque of DC1 for one electrical cycle compared to the baseline.

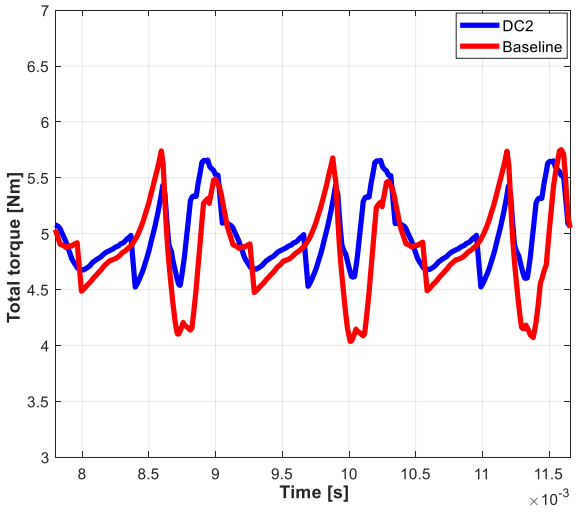

FIGURE 15. Total torque of DC2 for one electrical cycle compared to the baseline.

1.8% and a remarkable reduction of torque ripples by 23.8% when compared to the baseline design.

The utilization of MLA in motor design offers numerous benefits, such as a reduction in computational overhead. This approach effectively acts as a surrogate model for static and dynamic simulations, including the optimization process of the conduction angles. As a result, it leads to significant savings in computational time. To quantify the amount of time saved, we calculated and recorded the execution time of all the steps involved in obtaining the design candidates. It took a total of 2,000 minutes to obtain the 50 data points comprising the training dataset. Each individual data point necessitates 25 minutes for executing the static FEA model and generating the required lookup tables. Additionally, the MATLAB SIMULINK model, which includes the GA optimization of conduction angles, consumes 15 minutes for each data point. Then, the proposed method took approximately 10 minutes to learn the training data and generate 10,000 new data points. The studies presented in this work were conducted using a computer equipped with an Intel(R) Core (TM) i7-8700 CPU running at a speed of 3.20GHz and 32.0 GB of RAM. In comparison, using the conventional FEA and MATLAB method to get 10,000 points would take 400,000 minutes, which is a formidable computational cost. Therefore, the proposed method offers significant execution time savings.

VI. CONCLUSION AND FUTURE WORK

This study proposed a non-conventional optimization approach utilizing the BPNN to accurately map out the crucial SRM geometrical parameters, stator and rotor pole arc angles and their dynamic performance, including average

torque and torque ripples. The developed BPNN acts as a surrogate model, replacing both static and dynamic models, including GA optimization of the conduction angles. To enhance the training process, LM algorithm was implemented, ensuring efficient and rapid convergence while reducing network complexity. Using the developed approach, 10,000 design candidates for the considered 6/14 SRM were obtained. The optimal design was rigorously validated with high precision using FEA and SIMULINK analysis, establishing its reliability and superior performance. This proposed method showcases an improvement of 1.8% in the motor average torque and a remarkable reduction of 23.8% in torque ripples compared to the baseline design. Additionally, this method significantly reduced computational time and costs compared to conventional iterative techniques. Future research directions will consider the study of acoustic noise and vibration as they are out of the scope of this paper. Moreover, it will extend to consider other geometrical parameters such as the pole heights and taper angles.

ACKNOWLEDGMENT

The authors would like to thank POWERSYS Corporation for their support with JMAG software, and MathWorks for their support with MATLAB and Simulink software.

REFERENCES

[1] B. Bilgin, J. W. Jiang, and A. Emadi, *Switched Reluctance Motor Drives: Fundamentals to Applications*. Boca Raton, FL, USA: CRC Press, 2019.

[2] R. Vandana and B. G. Fernandes, "Design methodology for high performance segmented rotor switched reluctance motors," *IEEE Trans. Energy Convers.*, vol. 30, no. 1, pp. 11–21, Mar. 2015.

[3] M. Abdalmagid, E. Sayed, M. H. Bakr, and A. Emadi, "Geometry and topology optimization of switched reluctance machines: A review," *IEEE Access*, vol. 10, pp. 5141–5170, 2022.

[4] H. Zhang, W. Xu, S. Wang, Y. Huangfu, G. Wang, and J. Zhu, "Optimum design of rotor for high-speed switched reluctance motor using level set method," *IEEE Trans. Magn.*, vol. 50, no. 2, pp. 765–768, Feb. 2014.

[5] F. Sahin, H. B. Ertan, and K. Leblebicioglu, "Optimum geometry for torque ripple minimization of switched reluctance motors," *IEEE Trans. Energy Convers.*, vol. 15, no. 1, pp. 30–39, Mar. 2000.

[6] B. Mirzaeian, M. Moallem, V. Tahani, and C. Lucas, "Multiobjective optimization method based on a genetic algorithm for switched reluctance motor design," *IEEE Trans. Magn.*, vol. 38, no. 3, pp. 1524–1527, May 2002.

[7] H. Dhulipati, E. Ghosh, S. Mukundan, P. Korta, J. Tjong, and N. C. Kar, "Advanced design optimization technique for torque profile improvement in six-phase PMSM using supervised machine learning for direct-drive EV," *IEEE Trans. Energy Convers.*, vol. 34, no. 4, pp. 2041–2051, Dec. 2019.

[8] D. M. Ionel and M. Popescu, "Finite-element surrogate model for electric machines with revolving field—Application to IPM motors," *IEEE Trans. Ind. Appl.*, vol. 46, no. 6, pp. 2424–2433, Dec. 2010.

[9] W. Jiang, T. M. Jahns, T. A. Lipo, W. Taylor, and Y. Suzuki, "Machine design optimization based on finite element analysis in a high-throughput computing environment," in *Proc. IEEE Energy Convers. Congr. Exposit. (ECCE)*, Raleigh, NC, USA, Sep. 2012, pp. 869–876.

[10] P. Zhang, G. Y. Sizov, D. M. Ionel, and N. A. O. Demerdash, "Design optimization of spoke-type ferrite magnet machines by combined design of experiments and differential evolution algorithms," in *Proc. Int. Electric Mach. Drives Conf.*, Chicago, IL, USA, May 2013, pp. 892–898.

[11] B. Bilgin and M. Krishnamurthy, "An FEA/MATLAB based machine design tool for switched reluctance motors," in *Proc. IEEE Vehicle Power Propuls. Conf.*, Chicago, IL, USA, Sep. 2011, pp. 1–6.

[12] O. Zayed, M. Omar, M. Bakr, M. Narimani, A. Emadi, and B. Bilgin, "Switched reluctance motor design for an EV propulsion application," in *Proc. 47th Annu. Conf. IEEE Ind. Electron. Soc. (IECON)*, Toronto, ON, Canada, Oct. 2021, pp. 1–6.

[13] M. Omar, E. Sayed, M. Abdalmagid, B. Bilgin, M. H. Bakr, and A. Emadi, "Review of machine learning applications to the modeling and design optimization of switched reluctance motors," *IEEE Access*, vol. 10, pp. 130444–130468, 2022.

[14] J. Song, F. Dong, J. Zhao, H. Wang, Z. He, and L. Wang, "An efficient multiobjective design optimization method for a PMSLM based on an extreme learning machine," *IEEE Trans. Ind. Electron.*, vol. 66, no. 2, pp. 1001–1011, Feb. 2019.

[15] M. H. Mohammadi, T. Rahman, R. Silva, M. Li, and D. A. Lowther, "A computationally efficient algorithm for rotor design optimization of synchronous reluctance machines," *IEEE Trans. Magn.*, vol. 52, no. 3, pp. 1–4, Mar. 2016.

[16] H. Sahraoui, H. Zeroug, and H. A. Toliyat, "Switched reluctance motor design using neural-network method with static finite-element simulation," *IEEE Trans. Magn.*, vol. 43, no. 12, pp. 4089–4095, Dec. 2007.

[17] Z. Zhang, S. Rao, and X. Zhang, "Performance prediction of switched reluctance motor using improved generalized regression neural networks for design optimization," *CES Trans. Electr. Mach. Syst.*, vol. 2, no. 4, pp. 371–376, Dec. 2018.

[18] B. Howey, B. Bilgin, and A. Emadi, "Design of an external-rotor direct drive E-bike switched reluctance motor," *IEEE Trans. Veh. Technol.*, vol. 69, no. 3, pp. 2552–2562, Mar. 2020.

[19] B. Bilgin, A. Emadi, and M. Krishnamurthy, "Design considerations for switched reluctance machines with a higher number of rotor poles," *IEEE Trans. Ind. Electron.*, vol. 59, no. 10, pp. 3745–3756, Oct. 2012.

[20] S. Li, S. Zhang, T. G. Habetler, and R. G. Harley, "Modeling, design optimization, and applications of switched reluctance machines—A review," *IEEE Trans. Ind. Appl.*, vol. 55, no. 3, pp. 2660–2681, May/Jun. 2019.

[21] J. Dong, B. Howey, B. Danen, J. Lin, J. W. Jiang, B. Bilgin, and A. Emadi, "Advanced dynamic modeling of three-phase mutually coupled switched reluctance machine," *IEEE Trans. Energy Convers.*, vol. 33, no. 1, pp. 146–154, Mar. 2018.

[22] M. Bakr, *Nonlinear Optimization in Electrical Engineering With Applications in MATLAB*. London, U.K.: Institution of Engineering and Technology, 2013.

[23] Y. Cai, Y. Wang, H. Xu, S. Sun, C. Wang, and L. Sun, "Research on rotor position model for switched reluctance motor using neural network," *IEEE/ASME Trans. Mechatronics*, vol. 23, no. 6, pp. 2762–2773, Dec. 2018.

[24] R. Krishnan, *Switched Reluctance Motor Drives Modeling, Simulation, Analysis, Design, and Applications*. Boca Raton, FL, USA: CRC, 2001.

MOHAMED OMAR (Graduate Student Member, IEEE) received the B.Sc. degree (Hons.) in electrical engineering from the Shoubra Faculty of Engineering, Benha University, Cairo, Egypt, in 2011, and the M.Sc. degree in electrical engineering from Cairo University, Egypt, in 2017. He is currently pursuing the Ph.D. degree in electrical engineering with the McMaster Automotive Resource Centre (MARC), McMaster University, ON, Canada, in 2020. After the bachelor's degree, he was an Assistant Researcher with the Electronics Research Institute, Cairo. He is involved in an industrial project where he performs the design and testing of solid-state power converters (SSPC) for an aerospace application. His research interests include the design and modeling of switched reluctance motors using machine learning.

MOHAMED H. BAKR (Senior Member, IEEE) received the B.Sc. degree (Hons.) in electronics and communications engineering and the master's degree in engineering mathematics from Cairo University, Egypt, in 1992 and June 1996, respectively, and the Ph.D. degree from the Department of Electrical and Computer Engineering, McMaster University, in September 2000. In 1997, he was a student intern with Optimization Systems Associates (OSA) Inc. In November 2000, he joined the Computational Electromagnetics Research Laboratory (CERL), University of Victoria, Victoria, Canada, as an NSERC Post Doctoral Fellow. He received the Premier's Research Excellence Award (PREA) from the province of Ontario, Canada, in 2003. He also received an NSERC Discovery Accelerator Supplement (DAS) Award, in 2011. In 2014, he was a co-recipient of the Chrysler's Innovation Award for project on novel designs of hybrid cars. In 2020, he was a recipient of the Faculty Appreciation Award by the McMaster Engineering Society (MES). In April 2021, he was awarded the President's Award for Outstanding Contributions for Teaching and Learning from McMaster University. In July 2021, he was awarded a Distinguished Engineering Educator honorific from the Faculty of Engineering, McMaster University. He was also included in Stanford's list of the top 2% most cited scientists for the years 2020–2022. His research interests include optimization methods, computational electromagnetics, computer-aided design and the modeling of power circuits and motors, microwave circuits, THz, and photonic devices, nanotechnology, artificial intelligence and its applications, the smart analysis of high frequency structures, and efficient optimization using time/frequency domain methods. He is currently the Chair of the Department of Electrical and Computer Engineering, McMaster University. He has authored/coauthored over 290 journals and conference papers, two books on the optimization and CAD of high frequency structures, three book chapters on optimization, electromagnetic modeling, and artificial intelligence, and three patents.

ALI EMADI (Fellow, IEEE) received the B.S. and M.S. degrees (Hons.) in electrical engineering from the Sharif University of Technology, Tehran, Iran, in 1995 and 1997, respectively, and the Ph.D. degree in electrical engineering from Texas A&M University, College Station, TX, USA, in 2000. He is currently the Canada Excellence Research Chair Laureate of McMaster University, Hamilton, ON, Canada. He is also the holder of the NSERC/FCA Industrial Research Chair of Electrified Powertrains and the Tier I Canada Research Chair of Transportation Electrification and Smart Mobility. Before joining McMaster University, he was the Harris Perlstein Endowed Chair Professor of Engineering and the Director of the Electric Power and Power Electronics Center and Grainger Laboratories, Illinois Institute of Technology, Chicago, where he established research and teaching facilities and courses in power electronics, motor drives, and vehicular power systems. He was the Founder, the Chairperson, and the President of Hybrid Electric Vehicle Technologies Inc. (HEVT), a university spin-off company of Illinois Tech. He is also the President and the Chief Executive Officer of Enedym Inc. and Menlolab Inc.—two McMaster University spin-off companies. He is the principal author/coauthor of over 500 journals and conference papers and several books, including *Vehicular Electric Power Systems*, in 2003, *Energy Efficient Electric Motors*, in 2004, *Uninterruptible Power Supplies and Active Filters*, in 2004, *Modern Electric, Hybrid Electric, and Fuel Cell Vehicles* (Second Edition, 2009), and *Integrated Power Electronic Converters and Digital Control*, in 2009. He is also an Editor of the *Handbook of Automotive Power Electronics and Motor Drives*, in 2005 and *Advanced Electric Drive Vehicles*, in 2014. He is a Co-Editor of the *Switched Reluctance Motor Drives*, in 2018. He was the Inaugural General Chair of the 2012 IEEE Transportation Electrification Conference and Expo (ITEC) and he has chaired several IEEE and SAE conferences in the areas of vehicle power and propulsion. He was the founding Editor-in-Chief of IEEE TRANSACTIONS ON TRANSPORTATION ELECTRIFICATION, from 2014 to 2020.